Structural and frictional properties of graphene films on SiC(0001) studied by atomic force microscopy

T. Filleter[1] and R. Bennewitz[1,2,*]
[1]*Department of Physics, McGill University, Montreal, Quebec, Canada H3A 2T8*
[2]*INM—Leibniz Institute for New Materials, 66123 Saarbrücken, Germany*
(Received 8 October 2009; revised manuscript received 4 March 2010; published 6 April 2010)

Structural and frictional properties of single-layer and bilayer graphene films on a SiC(0001) substrate are studied by means of atomic force microscopy with atomic resolution. Friction on single-layer graphene is found to be a factor of two larger than on bilayer films for a variety of experimental situations. The friction contrast is found not to originate in differences in structural properties, in lateral contact stiffness, or in contact potential. The transition from atomic stick-slip friction to a regime of ultralow friction is found to occur at normal loads of 40 nN when the tip-sample interaction potential approaches 0.1–0.2 eV.

DOI: 10.1103/PhysRevB.81.155412 PACS number(s): 68.35.Af, 62.20.Qp, 68.37.Ps

I. INTRODUCTION

Carbon-based materials exhibit some of the most unique mechanical properties found in nature. The three-dimensional sp^3 bonding in diamond yields the hardest known material and the pseudo-two-dimensional sp^2 bonding in graphite yields one of the most effective solid lubricants. Graphite is composed of a stack of graphene layers weakly bonded in the third dimension by van der Waals bonds. Graphene is an emerging material and a possible candidate to advance microelectronics in a post-silicon era[1] due to its exotic electrical transport properties which derive from the Dirac-type behavior of charge carriers.[2–4] However, mechanical properties of graphene are also of interest, in particular, its lubricating properties as the building block of graphite.

Graphite has been one of the materials studied widely by friction force microscopy (FFM).[5–8] It has been instrumental in demonstrating many atomic-scale frictional phenomena. It was the material on which atomic stick-slip friction was observed by Mate *et al.*[5] in a pioneering study; it was used as a template to demonstrate the statistics of thermally activated slips in stick-slip motion;[8] and the rotation of its lattice with respect to the scanning tip revealed the phenomena of structural, or superlubricity.[7] The epitaxial growth of graphene on SiC allows the measurement of the tribological properties of graphite when reduced to its most fundamental thickness limit; ultrathin graphene sheets. Recently we studied single-layer and bilayer graphene films grown epitaxially on SiC and demonstrated that when the thickness of graphene films is reduced from bilayer films to single graphene layers friction increases by a factor of 2.[9] A reduction in friction due to graphene layers and a variation in friction between graphene layers of different thickness has also been found on a silicon oxide surface.[10] A decrease of atomic friction with growing number of graphene layers has been confirmed on silicon surfaces, even above micrometer-size holes.[11]

Here we report further studies of graphene films on SiC using both dynamic and static atomic force microscopy methods. The surface morphology and atomic structure of the films are first investigated using noncontact atomic force microscopy (nc-AFM). Friction force microscopy results are then presented which reveal atomic stick-slip frictional properties using different tip materials, ultralow friction at low loads, and the effects of an applied bias on friction. These detailed studies confirm that the friction contrast between single-layer and bilayer films cannot be explained by differences in structure, orientation, lateral contact stiffness, or electrostatic attraction. The friction contrast rather reveals an additional dissipation mechanism for single-layer graphene, presumably the electron-phonon coupling discovered by angle-resolved photoemission studies.[9]

II. EXPERIMENTAL

Single and bilayer graphene films were grown on the Si-terminated (0001) face of 6H-SiC using the thermal decomposition synthesis method. Films were prepared following procedures outlined for synthesis under both ultrahigh vacuum (UHV) (Ref. 12) and near atmospheric pressure[13] environmental conditions. After synthesis the samples were transferred through air and introduced into an ultrahigh vacuum chamber, and degassed at a temperature of 600 °C. The temperature during heating was monitored using an infrared pyrometer with an emissivity setting of 0.90.[12]

The films were characterized using a home-built multimode force microscope operated in both dynamic and static imaging modes.[14] The local film thickness of graphene layers was determined by means of Kelvin probe force microscopy which records contact potential difference maps; the thickness determination was confirmed by measurement of differences in the corrugation height of the films caused by the underlying surface reconstruction.[15] Single-crystal Si and polycrystalline diamond-coated rectangular AFM cantilevers with integrated tips (Nanosensors) were used for AFM measurements. The crystallites at the apex of diamond-coated tips have a much larger tip radius as compared to the Si tips (see Fig. 1). For nc-AFM measurements the first normal resonance frequency of the cantilevers was 63–300 kHz. The tip-sample distance was controlled by maintaining a constant frequency shift of the resonance while keeping the oscillation amplitude constant. Simultaneously with topography maps we have recorded maps of the cantilever excitation amplitude A_{exc} which is required to maintain constant ampli-

 ©2010 The American Physical Society

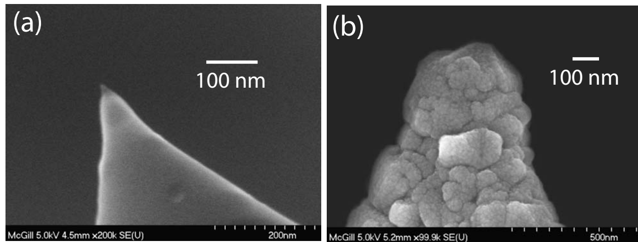

FIG. 1. Scanning electron microscopy images of the integrated tips of (a) Si and (b) diamond-coated Si AFM cantilevers used for AFM experiments.

tude. This signal reflects the damping of the cantilever oscillation in the course of tip-sample interaction. While a quantitative analysis of the signal is not straightforward due to the nonlinear nature of the interaction,[16] it provides an excellent tool to detect subtle differences in the local corrugation of surfaces because its distance characteristic is much steeper than that of the frequency shift.[17] Normal and lateral spring constants of individual cantilevers were calibrated using the geometrical beam calibration method.[18] For precision assessment some normal and lateral spring constants were additionally calibrated using the Sader calibration method,[19] which resulted in differences of less than 20% in all cases.

III. RESULTS AND DISCUSSION

A. Surface morphology and atomic structure: Noncontact AFM

In this section we compare the surface morphology of single-layer and bilayer graphene with the carbon-rich interface layer on top of the SiC substrate. Figures 2(a) and 2(b) show overview nc-AFM images of SiC surfaces covered with graphene films with a nominal thickness of <1 monolayer grown by thermal decomposition in UHV and argon environments, respectively. After heat treatment in UHV the SiC surface exhibits a high density of surface steps beneath the graphene films. The inset in Fig. 2(a) demonstrates that these SiC steps are oriented with hexagonal symmetry as a result of the hcp crystal structure. In contrast, and in agreement with scanning tunneling microscopy (STM)

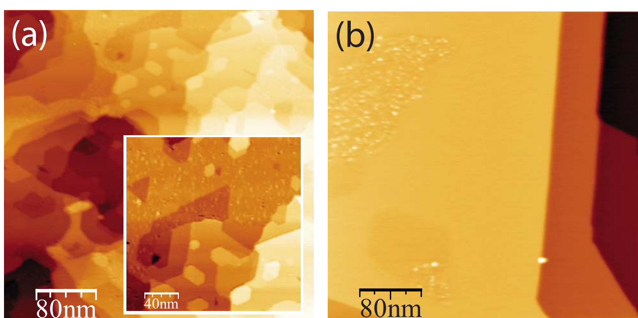

FIG. 2. (Color online) Noncontact mode AFM images of graphene films grown on SiC(0001) by thermal decomposition under (a) UHV conditions and (b) near atmospheric pressure conditions. The insert in (a) shows SiC steps beneath the graphene film with hexagonal step orientation.

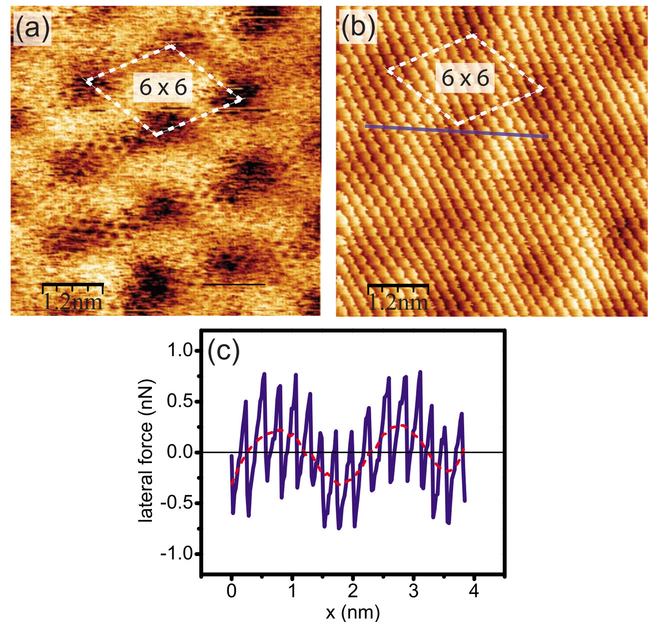

FIG. 3. (Color online) (a) Atomically resolved noncontact mode AFM image of a graphene film. (b) Atomic stick-slip lateral force map recorded on a graphene film. A corrugation with a 6×6 periodicity of the underlying SiC lattice is observed in both the nc-AFM topographic map and the lateral force map. (c) Cross section of the lateral force along the line indicated in (b). The dashed line shows the same profile after smoothing revealing that the superstructure adds a significant modulation to the offset of the lateral force.

studies,[13] the surface synthesized near atmospheric pressure exhibits a much smoother surface morphology. In both images, areas covered in the carbon-rich interface layer can be identified from a high density of adsorbates that probably remain from the exposure to air despite the degassing procedure. Areas covered with graphene are atomically clean as will be demonstrated by atomic-resolution images.

Several STM studies of epitaxially grown graphene films have demonstrated that the films exhibit a superstructure related to the underlying surface reconstruction of the SiC surface.[20–23] It is not clear, however, if the corrugation in STM is mostly of topographic nature or follows the electronic structure. Atomically resolved nc-AFM images recorded on graphene films reveal a corrugation with a 6×6 periodicity of the SiC lattice, consistent with the STM observations. Figure 3(a) shows an nc-AFM image in which the graphene unit cell is locally resolved. The same 6×6 corrugation is also observed in contact mode AFM imaging as demonstrated by the lateral force map recorded on a graphene film in Fig. 3(b). The atomic friction maps will be discussed in more detail in the following section.

STM studies have also shown that the corrugation caused by the superstructure is greater on single graphene layer films compared to bilayer films. This has previously been confirmed using AFM imaging.[15] Figure 4(a) shows an overview region of a sample surface covered in areas of interface layer (IFL), single-layer graphene (1LG), and bilayer graphene (2LG) which have been identified[15] from the simultaneously recorded contact potential map [Fig. 4(b)]. The

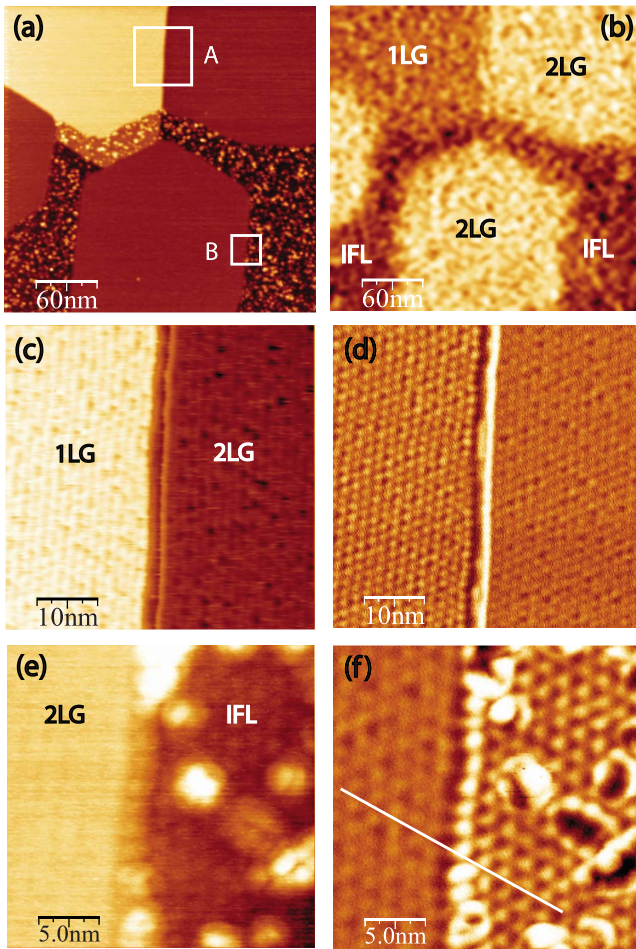

FIG. 4. (Color online) (a) Overview nc-AFM topography image (z scale: 0–0.7 nm) and (b) Contact potential difference map of a surface region covered in areas of IFL, 1LG, and 2LG. (c) Topography image (z scale: 0–0.8 nm) and (d) A_{exc} image recorded on the transition region between 1LG and 2LG at point A in (a). (e) Topography image (z scale: 0–0.6 nm) and (f) A_{exc} image recorded on the transition region between 2LG and IFL at point B in (a). The white line serves as a guide to the eye to demonstrate the absence of a lateral shift of the superstructure across the transition.

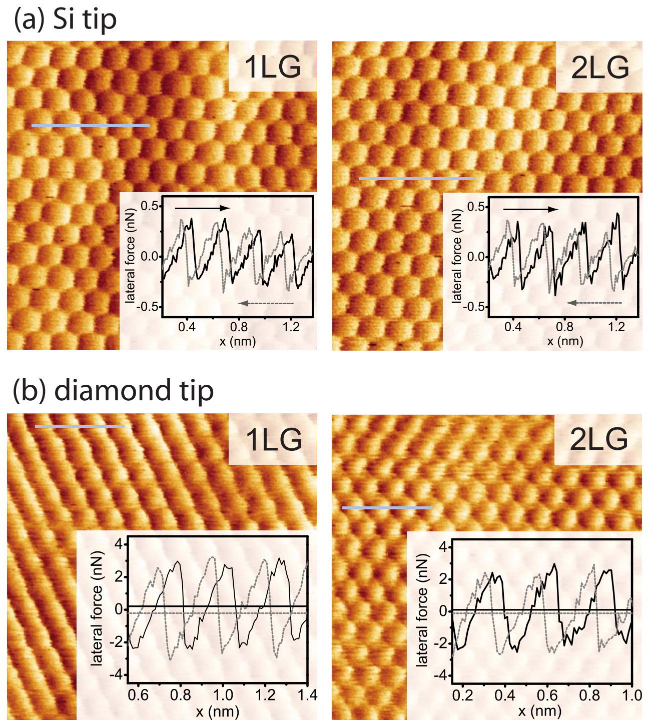

FIG. 5. (Color online) Lateral force maps and line profiles recorded on adjacent 1LG and 2LG films. (a) Image recorded using a silicon tip. (Image size: 3×3 nm^2, scan speed: 20 nm/s, normal load: 13 nN.) (b) Image recorded using diamond-coated tip. (Image size: 3×3 nm^2, scan speed: 20 nm/s, normal load: 181 nN.) Different loads have been chosen for silicon and diamond tips in order to account for the difference in tip radius (see Fig. 1) and to obtain a comparable contact pressure.

images in Fig. 4 have been recorded with a very sharp silicon tip, allowing for high resolution at the transitions between different layer thicknesses at the cost of higher noise in the contact potential difference map. As introduced in Sec. II, the weak 6×6 corrugation of the superstructure exhibits good contrast in the simultaneously recorded amplitude excitation signal (A_{exc}) in nc-AFM mode. Figures 4(c) and 4(d) show topography and A_{exc} images of the transition between 1LG and 2LG films at position A in Fig. 4(a). The A_{exc} signal exhibits a clear 6×6 pattern on both the 1LG and 2LG region of the sample with higher contrast on the 1LG region. We can also confirm, from AFM images, that the 6×6 superstructure is present on the IFL region of the sample as demonstrated in Figs. 4(e) and 4(f). The contrast in the A_{exc} signal is much higher on the IFL than on the 2LG layer. A straight line in Fig. 4(f) furthermore reveals that there is no lateral shift in the superstructure across the transition which would indicate a geometric interference effect as source of the 6×6 corrugation.[24] We conclude that the 6×6 superstructure observed on 1LG and 2 LG films is a truly topographic corrugation caused by the reconstruction of the SiC surface and weakened with increasing film thickness.

B. Frictional properties of films: Friction force microscopy

1. Atomic stick-slip friction

The lateral force acting on a FFM tip sliding over a crystalline lattice is typically modulated in a saw-tooth fashion with the periodicity of the surface lattice. This atomic stick-slip friction process has been previously demonstrated many times on bulk graphite surfaces.[5,7,8] On graphite, the tip is found to stick in energetic minima positioned at the hollow sites of the honeycomb lattice yielding a stick-slip pattern with the periodicity of the unit cell, not the individual atomic sites of the carbon atoms.[8]

Similar stick-slip patterns have been previously observed on both 1LG and 2LG films,[9] and are demonstrated again in Fig. 5 for both sharp Si tips and diamond-coated tips. Similar to graphite, the periodicity of the stick slip reproduces the top-surface honeycomb lattice of the hollow sites on both layer thicknesses. This is in contrast to atomic-resolution imaging with STM, which probes the electronic structure of the surface and reveals stacking differences between 1LG and 2LG.[23] STM studies of epitaxial bilayer graphene have

shown that Bernal stacking is most often observed, in this case each hollow site of the top graphene layer lies above an α atom of the graphene sheet below, whereas for epitaxially grown 1LG on SiC the bonding configuration below the hollow site is unclear. The underlying interface layer has a very similar structure to graphene.[25] Our results show that any differences in bonding to the underlying layer do not affect the periodicity of the stick-slip pattern observed in friction experiments on 1LG and 2LG.

Lateral force maps of graphene layers on SiC exhibit one distinct difference compared to graphite. A modulation in the lateral force is observed [see Fig. 3(b)] with the same 6×6 periodicity already observed in the corrugation of the films. Observations of a modulation in the lateral force measured on a corrugated film have been reported for KBr films grown on NaCl (Ref. 26) and on Cu(100).[24] However, for the KBr films a significant modulation in the amplitude of the stick-slip traces was found whereas for graphene films we find minimal modulation in amplitude. Instead a significant variation is found in the average lateral force within the stick-slip pattern of a single scan line [see Fig. 3(c)]. The smoothed line in the figure better reveals this offset, the exact nature of which is unclear at this time. An explanation may include the fact that the amplitude modulation of stick slip on KBr films reflects a lattice mismatch in heteroepitaxy while the offset modulation of stick slip on graphene films is caused by a reconstruction of the substrate surface. It should be noted that both cases exhibit a combined effect of a modulated amplitude and offset, however, in the case of graphene films the offset modulation dominates.

The orientation of the lattice for both layer thicknesses can also be compared in Fig. 5. Here, and in all other cases which we studied, the adjacent 1LG and 2LG areas have the same crystalline orientation. This is expected, as it has been suggested that these graphene films grow continuously over substrate steps and that the transition between 1LG and 2LG is due to the insertion of an underlying layer.[23] The orientation of the film with respect to the scan direction in friction experiments is critical because the commensurability between the tip and sample structure has a significant influence on friction.[7]

In a recent study we reported that friction, i.e., the average lateral force, is twice on 1LG compared to 2LG.[9] This observation is demonstrated again using new data of measurements with diamond tips in Fig. 6. The filled squares show that the ratio between friction on 1LG and 2LG is always around a value of 2. For comparison, open squares show the corresponding ratio for measurements taken with silicon tips, where the median value of the ratio is 1.81. The scatter in the silicon tip data is significant but the trend is confirmed. Friction is always found to be higher on 1LG than on 2LG in almost all cases by a factor between 1.5 and 2.5. Friction data recorded with the silicon tip are subject to higher noise because the normal and lateral forces for the small contact of the sharp tip are much smaller. Furthermore, even smallest changes in the tip structure when moving forth and back between patches of 1LG and 2LG will influence the results greatly while the blunter diamond-coated tips always exhibit a more stable behavior.

In this section we have already shown that crystallographic structure and orientation as seen by the FFM are the same on 1LG and 2LG. A further parameter which can influence friction is the lateral contact stiffness. It can be derived from the slope of the sticking phase in lateral force curves like the ones shown in the inserts in Fig. 5. The lateral contact stiffness is larger for diamond-coated tips as compared to silicon tips and it increases with load. In both cases the increase in lateral contact stiffness reflects an increase in the contact size.[27] However, we find that at a given load the lateral contact stiffness is always the same for 1LG and 2LG. This is demonstrated by the filled triangles in Fig. 6 for diamond-coated tips. Unfortunately, the scatter in the data did not allow a similar analysis for the silicon tips, such that load dependence of atomic stick slip and of the average lateral force could be evaluated while moving between 1LG and 2LG areas.

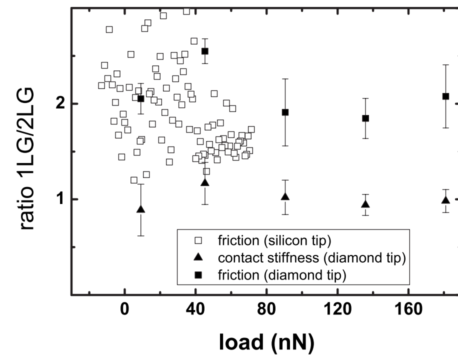

FIG. 6. Ratio of friction on 1LG and 2LG as a function of load (squares) and ratio of the contact stiffness on 1LG and 2LG (triangles). Open symbols represent data recorded with a silicon tip, filled symbols data of a diamond tip. Error bars represent the standard deviation in the averaging of 250 scan lines. They do not reflect occasional changes in the atomic configuration of the atomic tip structure upon moving to new spots or changing the load, which are assumed to dominate the scatter in the data for the sharp silicon tips.

However, with very sharp Si tips the contact area becomes so small that a 1LG area, the transition area, and a 2LG area can be imaged within a single scan frame. Such measurements require both a high data acquisition rate (25 kHz) and high spatial resolution (1792×1792 points per full frame) in order to resolve atomic stick slip on both layer thicknesses. Figure 7(a) shows a lateral force map recorded over a transition between 1LG and 2LG at an underlying SiC step. This

FIG. 7. (Color online) (a) High spatial resolution lateral force map recorded on a sample region with a transition between 1LG and 2LG films. (Image size: 25×5.7 nm^2.) (b) Magnification of data on the 1LG region in (a). (c) Magnification of data on the 2LG region in (a).

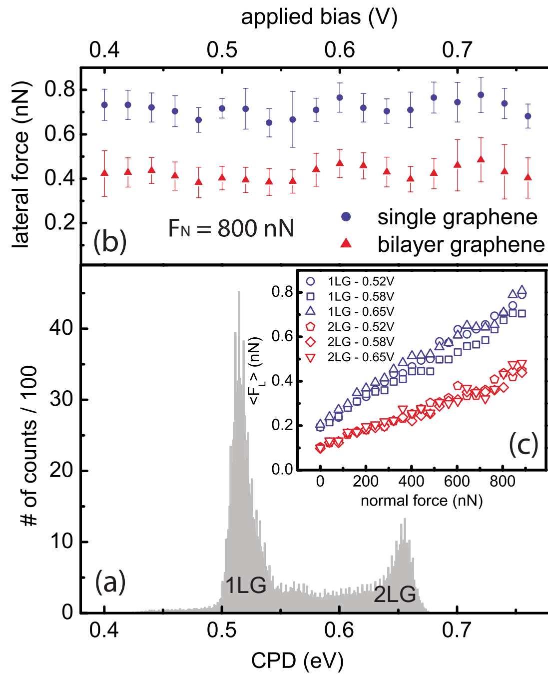

FIG. 8. (Color online) (a) Histogram of contact potential differences with respect to the diamond tip recorded over a transition region from 1LG to 2LG. (b) Friction force as a function of tip-sample bias on the same 1LG and 2LG sample regions at a normal load of 800 nN. (c) Friction force vs normal load recorded on the same sample area for three different tip-sample biases. Errors in the friction data (not shown) range from approximately 0.04–0.06 nN and show an increasing trend with normal load.

experiment allows us to determine the contact stiffness on 1LG and 2LG areas within the same scan line, definitely ensuring that there is no influence of a changing tip. From portions of the lateral force map [Figs. 7(b) and 7(c)] taken far from the transition region, the contact stiffness was again determined to be equal on both layers. The contact stiffness was 10.8 ± 0.2 N/m on 1LG and 10.8 ± 0.3 N/m on 2LG.

2. Bias dependence of friction

Kelvin probe microscopy experiments have demonstrated that there is a difference in the local contact potential between 1LG and 2LG.[15] This leads to a difference in the electrostatic force acting between the probing tip and the two different surface regions at constant tip-sample bias. The difference in electrostatic force is also present in contact mode AFM experiments and may lead to variations in friction between 1LG and 2LG as a result of a different effective normal load. In order to identify any effect of the contact potential difference on friction, measurements of the average lateral force on 1LG and 2LG films have been conducted using a diamond tip at varying tip-sample biases. Figure 8(a) shows a histogram of contact potential differences with respect to the diamond tip for a surface area with a transition from 1LG to 2LG. After recording the contact potential, local friction measurements were conducted across the same region. Figure 8(b) shows the friction force measured on 1LG and 2LG regions as a function of tip-sample bias at a normal load of 800 nN. While the applied bias may have a small effect on the absolute friction force, there is no significant change in the ratio of friction forces between 1LG and 2LG. Figure 8(c) shows the load dependence of friction measured at three values of applied bias; 0.52 V, 0.65 V (where the contact potential for 1LG and 2LG is compensated, respectively) as well as 0.58 V (the center between the two values). Biases of 0.52 V and 0.65 V correspond to minimal electrostatic forces acting between the tip and the 1LG and 2LG film layers, respectively. The results demonstrate that there is no significant influence of the bias on friction within the range of the contact potential variation between tip on the different layer thicknesses. We conclude that the friction contrast between 1LG and 2LG is neither an electrostatic force effect nor an electronic effect caused, for example, by a carrier density variation through the contact potential difference between 1LG and 2LG.

3. Transition from continuous sliding to stick-slip friction

Experimental situations in which states of ultralow friction can be attained through external control have recently attracted significant attention. For example, friction on graphite has been switched on and off by changing the orientation of a sliding graphite flake.[7] Friction arising from dissipation in atomic stick-slip processes has been suppressed by dynamic actuation of the sliding contact.[28] A transition from a continuous sliding state with ultralow friction at low loads to the onset of stick-slip sliding with friction at higher loads has been reported for NaCl(100) surfaces and explained within the framework of the Tomlinson model.[29] This transition from smooth sliding to stick-slip behavior depends on the relation between the elastic energy arising from the lateral contact stiffness and the corrugation of the lateral potential describing the interaction between tip and sample, where the latter could be varied through the applied normal load. The transition has also been observed on KBr films grown on NaCl where the height of the lateral potential varies across a superstructure.[26]

Here we demonstrate this load-dependent transition for an ultrathin film composed of a bilayer of graphene. Figures 9(a) and 9(b) show lateral force maps recorded using a Si tip in the same region of a 2LG film at normal loads of 4 nN and 78 nN, respectively. From the lateral force profiles [Fig. 9(c)] along the lines indicated in the force maps, two distinct sliding regimes are observed. In Fig. 9(a) the tip continuously slides over the surface in a ultralow friction regime, whereas in Fig. 9(b) stick-slip instabilities are observed together with a large hysteresis in the lateral force between forward and backward scan, which corresponds to significant energy dissipation. Figure 9(d) reveals that the transition from the ultralow friction regime to stick-slip sliding occurs at approximately 40 nN.

The transition observed on graphene occurs at a much higher normal load than for NaCl ($\sim$1 nN) (Ref. 29) although similar tips have been used. The onset of stick slip occurs when $\eta = \frac{2\pi^2 E_0}{ka^2}$ becomes greater than 1 with E_0, k, and a the energy corrugation, effective stiffness, and lattice spacing, respectively. This transition condition should occur at a similar value of E_0 suggesting that at the same normal load

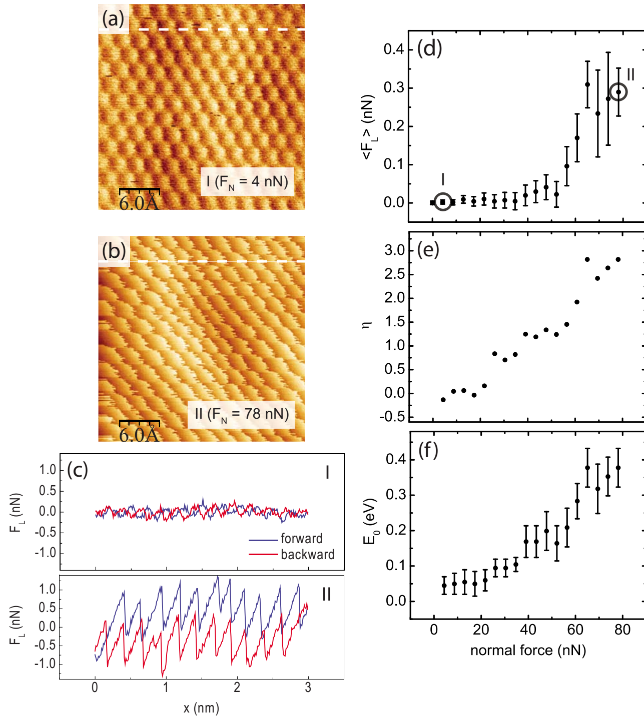

FIG. 9. (Color online) Atomic stick-slip friction maps recorded using a Si tip on 2LG at normal loads of (a) 4 nN and (b) 78 nN. (c) Lateral force loops recorded along the lines indicated in (a) and (b) demonstrating a transition from continuous sliding to stick-slip behavior. (d) Friction as a function of normal load determined from lateral force maps similar to (a) and (b). (e) Parameter η as a function of normal load. Note that the point $\eta=1$ corresponds to the transition to stick-slip behavior. (f) Potential corrugation E_0 as a function of normal load.

the Si tip-sample interaction potential is 40 times lower on graphene than on NaCl. The effective stiffness observed in experiments is roughly four times higher and the lattice spacing is a factor of two lower for graphene, therefore ka^2 is approximately equal for experiments on graphene and NaCl. The transition is indeed found at a similar value of E_0. Figures 9(e) and 9(f) shows the load dependence of η and E_0, respectively. The energy corrugation E_0 is determined from the maxima points of friction loops such as plotted in Fig. 9(c). The determination of η is difficult for very low loads, where $\eta<1$ as the slope of the sticking part is difficult to determine. However, the transition to stick slip and the onset of friction is observed in Fig. 9(d) at a corresponding value of $\eta=1$ as expected. From Fig. 9(f) we then find that the transition occurs at a potential corrugation of 0.1–0.2 eV, similar to observations on NaCl. To date we have not measured this transition on a 1LG film. However, we expect a similar transition and it would be interesting to compare the energy potential corrugation between 1LG and 2LG in future work.

IV. CONCLUSION

The structure of single-layer and bilayer films of graphene on SiC(0001) has been resolved by high-resolution noncontact AFM and FFM. The modulation of the graphene films by the reconstruction of the SiC surface exhibits the same features as in STM. We therefore conclude that the modulation is of topographic rather than electronic nature. In contrast to STM, the atomic structure observed by FFM is identical for the single-layer and the bilayer graphene films. While STM detects the lateral electronic structure of the stacking of graphene sheets, FFM results are fully dominated by the structure of the top layer.

We find an increase in friction by a factor of about 2 on single-layer graphene compared two bilayer graphene. This difference is found for a variety of experimental situations: for a wide range of normal loads, for silicon and diamond-coated tips, and at different bias voltages compensating differences in contact potential. Variations in parameters which typically cause friction contrasts can be excluded for single-layer and bilayer graphene. The structure of atomic stick-slip maps as well as the crystalline orientation are the same. We also find that the contact potential differences do not influence the friction contrast. Most important, the lateral contact stiffness does not vary between layer thicknesses. If the friction contrast of a factor of 2 were a consequence of a factor of 2 in the lateral potential barrier, the lateral contact stiffness would show a significant difference.[29] Consequently, the friction contrast is believed to originate in differences in the dissipation mechanism which affect the dynamics of the stick-slip motion. It has been suggested that the contrast in the stick-slip dynamics is related to a contrast in the electron-phonon coupling discovered by angle-resolved photoemission experiments.[9] The results presented in this paper do not provide direct evidence for the role of electron-phonon coupling in atomic friction. They do, however, exclude that the observed friction contrast originates in differences of structure, contact potential, or lateral contact stiffness as discussed above.

Finally, a regime of ultralow friction is demonstrated at low loads, where the dissipative stick-slip motion changes into a smooth sliding behavior. The transition occurs at a lateral potential barrier of about 0.2 eV, similar to a previously reported experiment on NaCl where similar AFM tips had been used. The normal load corresponding to this lateral potential barrier is a factor of 40 higher on graphene as compared to NaCl.

ACKNOWLEDGMENTS

This work was supported by the Canada Foundation of Innovation and NSERC. Sample preparation by and fruitful discussions with Thomas Seyller (University of Erlangen) are gratefully acknowledged.

*roland.bennewitz@inm-gmbh.de

[1] C. Berger, Z. Song, X. Li, X. Wu, N. Brown, C. Naud, D. Mayou, T. Li, J. Hass, A. N. Marchenkov, E. H. Conrad, P. N. First, and W. A. de Heer, Science **312**, 1191 (2006).
[2] K. S. Novoselov, A. K. Geim, S. V. Morozov, D. Jiang, M. I. Katsnelson, I. V. Grigorieva, S. V. Dubonos, and A. A. Firsov, Nature (London) **438**, 197 (2005).
[3] Y. Zhang, J. W. Tan, H. L. Stormer, and P. Kim, Nature (London) **438**, 201 (2005).
[4] K. S. Novoselov, A. K. Geim, S. V. Morozov, D. Jiang, Y. Zhang, S. V. Dubonos, I. V. Grigorieva, and A. A. Firsov, Science **306**, 666 (2004).
[5] C. M. Mate, G. M. McClelland, R. Erlandsson, and S. Chiang, Phys. Rev. Lett. **59**, 1942 (1987).
[6] U. D. Schwarz, O. Zwörner, P. Köster, and R. Wiesendanger, Phys. Rev. B **56**, 6987 (1997).
[7] M. Dienwiebel, G. S. Verhoeven, N. Pradeep, J. W. M. Frenken, J. A. Heimberg, and H. W. Zandbergen, Phys. Rev. Lett. **92**, 126101 (2004).
[8] A. Schirmeisen, L. Jansen, and H. Fuchs, Phys. Rev. B **71**, 245403 (2005).
[9] T. Filleter, J. L. McChesney, A. Bostwick, E. Rotenberg, K. V. Emtsev, T. Seyller, K. Horn, and R. Bennewitz, Phys. Rev. Lett. **102**, 086102 (2009).
[10] H. Lee, N. Lee, Y. Seo, J. Eom, and S. Lee, Nanotechnology **20**, 325701 (2009).
[11] C. Lee, X. Wei, Q. Li, R. W. Carpick, J. W. Kysar, and J. Hone, Phys. Status Solidi B **246**, 2562 (2009).
[12] I. Forbeaux, J.-M. Themlin, and J.-M. Debever, Phys. Rev. B **58**, 16396 (1998).
[13] K. V. Emtsev, A. Bostwick, K. Horn, J. Jobst, G. L. Kellogg, L. Ley, J. L. McChesney, T. Ohta, S. A. Reshanov, J. Roehrl, E. Rotenberg, A. K. Schmid, D. Waldmann, H. B. Weber, and T. Seyller, Nature Mater. **8**, 203 (2009).
[14] L. Howald, E. Meyer, R. Lüthi, H. Haefke, R. Overney, H. Rudin, and H.-J. Güntherodt, Appl. Phys. Lett. **63**, 117 (1993).
[15] T. Filleter, K. V. Emtsev, T. Seyller, and R. Bennewitz, Appl. Phys. Lett. **93**, 133117 (2008).
[16] H. Hug and A. Baratoff, in *Noncontact Atomic Force Microscopy, NanoScience And Technology*, edited by S. Morita, R. Wiesendanger, and E. Meyer (Springer, Berlin, 2002), pp. 395–432.
[17] C. Loppacher, R. Bennewitz, O. Pfeiffer, M. Guggisberg, M. Bammerlin, S. Schär, V. Barwich, A. Baratoff, and E. Meyer, Phys. Rev. B **62**, 13674 (2000).
[18] E. Meyer, H. Hug, and R. Bennewitz, *Scanning Probe Microscopy: The Lab on a Tip* (Springer-Verlag, Berlin, 2004).
[19] C. Green, J. Lioe, H. Cleveland, R. Proksch, P. Mulvaney, and J. Sader, Rev. Sci. Instrum. **75**, 1988 (2004).
[20] C. Riedl, U. Starke, J. Bernhardt, M. Franke, and K. Heinz, Phys. Rev. B **76**, 245406 (2007).
[21] P. Mallet, F. Varchon, C. Naud, L. Magaud, C. Berger, and J.-Y. Veuillen, Phys. Rev. B **76**, 041403(R) (2007).
[22] G. M. Rutter, J. N. Crain, N. P. Guisinger, T. Li, P. N. First, and J. A. Stroscio, Science **317**, 219 (2007).
[23] P. Lauffer, K. V. Emtsev, R. Graupner, T. Seyller, L. Ley, S. A. Reshanov, and H. B. Weber, Phys. Rev. B **77**, 155426 (2008).
[24] T. Filleter, W. Paul, and R. Bennewitz, Phys. Rev. B **77**, 035430 (2008).
[25] K. V. Emtsev, F. Speck, T. Seyller, L. Ley, and J. D. Riley, Phys. Rev. B **77**, 155303 (2008).
[26] S. Maier, E. Gnecco, A. Baratoff, R. Bennewitz, and E. Meyer, Phys. Rev. B **78**, 045432 (2008).
[27] R. Carpick, D. Ogletree, and M. Salmeron, Appl. Phys. Lett. **70**, 1548 (1997).
[28] A. Socoliuc, E. Gnecco, S. Maier, O. Pfeiffer, A. Baratoff, R. Bennewitz, and E. Meyer, Science **313**, 207 (2006).
[29] A. Socoliuc, R. Bennewitz, E. Gnecco, and E. Meyer, Phys. Rev. Lett. **92**, 134301 (2004).